Journal of *Marine Science and Engineering*

MDPI

Article

Hydrodynamic and Trim Analysis of a Dihedral Bulbous Bow on a Longliner Hull

Héctor Rubén Díaz Ojeda [1,*], Yifu Zhang [2,3,*], Stephen Turnock [2] and Francisco Pérez Arribas [4]

[1] Instituto Universitario de Sistemas Inteligentes y Aplicaciones Numéricas en Ingeniería, Universidad de Las Palmas de Gran Canaria, Campus de Tafira, 35017 Las Palmas de Gran Canaria, Spain
[2] Maritime Engineering, University of Southampton, Boldrewood Campus, Southampton SO16 7QF, UK; s.r.turnock@soton.ac.uk
[3] High Performance Computing (HPC) Team, University of Southampton, Highfield Campus, Southampton SO17 1BJ, UK
[4] Departamento de Arquitectura, Construcción y Sistemas Oceánicos y Navales, Universidad Politécnica de Madrid, Calle Ramiro de Maeztu 7, 28040 Madrid, Spain; francisco.perez.arribas@upm.es
* Correspondence: hectorruben.diaz@ulpgc.es (H.R.D.O.); yifu.zhang@soton.ac.uk (Y.Z.)

Abstract

This study evaluates the hydrodynamic performance of a displacement-type FAO longliner fishing vessel fitted with a surface-piercing dihedral bulbous bow. Unlike conventional submerged bulbs, this configuration partially emerges at the free surface. Hydrodynamic behaviour was analysed under heavy- and light-load conditions using both computational and experimental fluid dynamics. Results show that the dihedral bulb significantly reduces total resistance beyond a critical speed of approximately 6 knots, whilst also affecting dynamic trim and vertical hydrodynamic forces. Full-scale effective power was estimated by extrapolating model results according to ITTC procedures. This study confirms that dihedral bulbous bows are well suited for retrofit applications on small fishing vessels under 20 m in length, achieving maximum resistance reductions of about 18% at higher speeds. These gains translate into notable fuel savings and reduced greenhouse gas emissions, making the retrofit both economically and environmentally advantageous.

Keywords: dihedral bulbous bow; fishing vessel hydrodynamics; resistance prediction; model–ship extrapolation; EFD vs. CFD

1. Introduction

A polyhedral bulbous bow is a distinctive bulb configuration characterised by planar faceted surfaces that extend above the waterline rather than remaining fully submerged beneath it. This geometry superficially resembles the axe-bow or X-bow configurations found on certain offshore vessels, occasionally leading to confusion with wave-piercing bow forms. However, the defining feature of polyhedral bulbs is the presence of pronounced chine lines along the faceted surfaces, which serve dual purposes: they simplify fabrication through developable surface geometry, and they facilitate retrofit installation on vessels not originally designed with bulbous bows. For this reason, polyhedral bulbs are frequently designated as added or retrofit bulbous bows in the literature. The chine lines are not merely constructional conveniences; they fundamentally influence the hydrodynamic performance of the bow through modification of flow separation and pressure distribution.

The polyhedral configuration is readily identifiable and may be either incorporated during initial vessel design or retrofitted subsequently as a performance enhancement

Academic Editor: Zhi Zong

Received: 18 December 2025
Revised: 9 February 2026
Accepted: 12 February 2026
Published: 17 February 2026

modification. Previous investigations have demonstrated that this bulb type can effectively reduce resistance in traditional fishing vessels, yielding corresponding reductions in fuel consumption and greenhouse gas emissions [1,2]. Fishing vessels represent a particularly compelling application domain, as their hull forms exhibit substantial variability depending on geographical operating region, target species, fishing methods, and local design traditions—in marked contrast with the highly standardised designs characteristic of large merchant vessels. This heterogeneity frequently results in bespoke hull forms developed through empirical evolution rather than systematic hydrodynamic series. Even when systematic parent hull series exist, supplementary analyses are typically required to identify opportunities for resistance reduction and performance optimisation, as evidenced by numerous studies in the literature [3–5]. Within this context, bulbous bow modifications represent pragmatic interventions, as they can be implemented without the extensive structural redesign or costly reconstruction that wholesale hull form alterations would necessitate. Consequently, if the resistance reduction potential of a particular bulb geometry can be convincingly demonstrated, its practical implementation becomes relatively straightforward compared with more invasive structural modifications affecting the parent hull.

Traditional approaches to hydrodynamic design and performance prediction have historically relied upon systematic model series, regression-based empirical formulations, or direct towing tank experimentation—methodologies constrained by the computational capabilities available during their development [6,7]. Contemporary naval architecture increasingly employs computational fluid dynamics (CFD) as a standard design tool [4,8,9], enabling systematic evaluation of numerous geometric configurations during preliminary design or retrofit feasibility studies within broader hull form optimisation frameworks [9].

Contemporary naval architecture increasingly employs computational fluid dynamics (CFD) as a standard design tool [4,8], enabling systematic evaluation of numerous geometric configurations during preliminary design or retrofit feasibility studies. This computational capability is particularly valuable for bulbous bow optimisation, where performance is sensitively dependent upon geometric parameters including immersion depth, longitudinal position, sectional area distribution, and volumetric displacement. Experimental evaluation of multiple bulb configurations through physical model testing would be economically prohibitive, whilst empirical prediction methods such as Holtrop–Mennen formulations lack the geometric resolution necessary to discriminate between alternative bulb designs. Modern design methodologies therefore typically combine limited towing tank experiments for validation purposes with extensive CFD parametric investigations to identify promising design candidates, as recommended by recent ITTC guidelines for resistance and propulsion prediction [9]. These integrated approaches form part of broader hull form optimisation strategies increasingly employed across the maritime industry to enhance energy efficiency and reduce environmental impact [7,10]. Given that ship resistance and installed power represent fundamental performance metrics with direct economic and environmental implications, accurate prediction across the operational speed range remains an essential requirement [11].

The present investigation examines the integration of a specific polyhedral bulb configuration—designated the dihedral bulbous bow—onto an artisanal longliner fishing vessel design published by the Food and Agriculture Organization (FAO). Whilst polyhedral bulb concepts were initially proposed several decades ago, their potential for resistance reduction remains highly relevant, particularly for small-scale fishing operations where modest efficiency improvements yield disproportionate economic benefits. Although previous studies have demonstrated the applicability of polyhedral bulbs to certain fishing vessel types, significant knowledge gaps persist regarding the underlying fluid dynamic

mechanisms responsible for resistance reduction, and regarding the operational conditions (speed, displacement, trim) under which performance benefits are realised. Additional hydrodynamic data for displacement-type fishing vessels are therefore required to establish design guidelines and operational envelopes for effective bulb implementation.

The research programme described herein evolved from fundamental hydrodynamic investigation to practical engineering application. Initial experiments were conducted at model scale in towing tank facilities, with the results validated and extended through complementary CFD analyses. Subsequently, the validated design was implemented on a full-scale operational vessel, providing an opportunity to assess real-world performance and to verify model-scale predictions. Therefore, the novelty of this research resides in the comparative, research-oriented assessment of the experimental and numerical components of the ship's hydrodynamics, and in their direct transfer to operational reality through implementation in a real case study. As a result, the present work goes beyond a purely academic investigation and constitutes applied research with direct engineering relevance.

Moreover, the data obtained provide novel insights into lift generation, trim behaviour, and the hydrodynamic influences of this type of dihedral bulb, which are currently not considered in a significant portion of FAO vessels or artisanal fishing vessels when aiming to reduce resistance to forward motion. In particular, this study contributes to identifying the appropriate operating point and loading conditions under which such bulbous designs are most effectively implemented.

This paper is structured as follows: Section 2 presents the vessel characteristics and bulb geometry, Section 3 describes the experimental and numerical methodologies employed, Section 4 presents validation results and performance comparisons, and Section 6 discusses the findings and their practical implications. The hydrodynamic analysis encompasses not only longitudinal resistance, but also vertical lift forces and dynamic trim behaviour associated with bulb integration, as trim modifications can substantially influence overall performance through changes in wetted surface area and propeller immersion. Model-scale results are extrapolated to full scale following ITTC guidelines, enabling estimation of effective power requirements and fuel consumption for representative light-load and heavy-load conditions corresponding to outbound transit to fishing grounds and loaded return to port, respectively. These power predictions facilitate economic feasibility assessment of bulb retrofit implementation, providing quantitative indicators for investment payback analysis and operational cost–benefit evaluation. This study concludes with a synthesis of key findings and recommendations for practical application.

2. Problem Description

This investigation examines the hydrodynamic performance of a novel class of developable bulbous bows designated dihedral bows. These bow configurations evolved from polyhedral bulb concepts originally introduced for small vessel applications during the 1990s. The dihedral geometry comprises two planar developable surfaces, designed following established methodology that accounts for material fabrication constraints whilst incorporating the hull's existing chine line geometry to ensure smooth geometric transition between the bulb and parent hull [2].

The present study evaluates dihedral bow performance through combined experimental fluid dynamics (EFD) towing tank testing and computational fluid dynamics (CFD) simulation in calm water conditions. Performance of the modified hull is benchmarked against the baseline configuration without bulbous bow, with particular emphasis on quantifying the hydrodynamic effects attributable to the dihedral bow geometry. The experimental programme encompasses model-scale testing at a geometric scale ratio of $\lambda = 6.5$ across two representative loading conditions and a Froude number range extending

to Fr = 0.45, corresponding to operational speeds typical of artisanal longliner vessels. The model geometries are derived from as-built vessel lines, ensuring that findings are directly applicable to practical retrofit implementation decisions for existing vessels.

The baseline hull geometry employed in this investigation is an FAO (Food and Agriculture Organization) reference design for small-scale longliner fishing vessels, as documented in the publicly available FAO vessel design repository [12,13]. The original hull lines are presented in Figure 1, showing the body plan, half-breadth plan, and profile of the unmodified configuration. This baseline geometry was subsequently modified through integration of the dihedral bulbous bow, with the resulting modified hull lines documented in Reference [14], which provides comprehensive details regarding the full-scale implementation on operational longliner vessels in the Sri Lankan fishing fleet. The FAO design serves as parent hull for more than 4000 longliner vessels currently operating in Sri Lankan waters, rendering performance improvements of even modest magnitude economically and environmentally significant at fleet scale. The main dimensions ans characteristics of the vessel are summarised in Table 1.

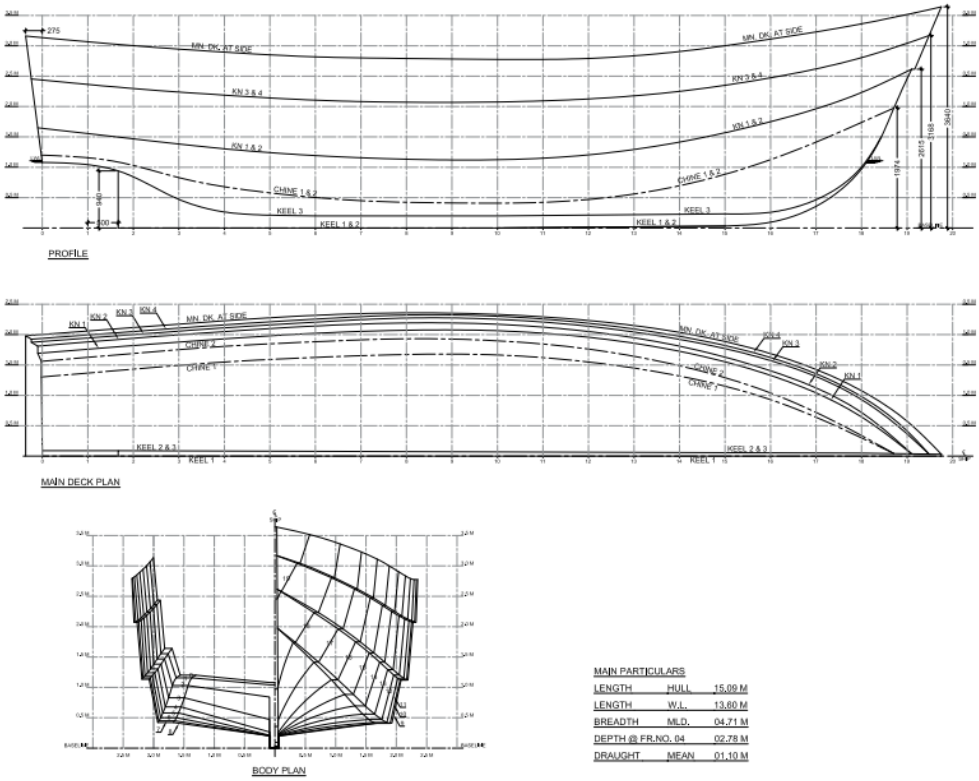

Figure 1. Lines plan of the fishing vessel including profile view, main deck plan, and body plan obtained from FAO. Main particulars are also indicated: hull length, 15.09 m; waterline length, 13.80 m; breadth, 4.71 m; depth, 2.78 m; and mean draught, 1.10 m.

Table 1. Main characteristics of the FAO longliner vessel.

Parameter	Value
Vessel type	Longliner
Length overall (LOA)	15.09 m
Maximum hull beam	4.71 m
Design draft	1.10 m
Depth	2.78 m
Displacement	35 tonnes
Construction material	GRP

Figure 2 illustrates the principal particulars and hydrostatic characteristics of the two loading conditions examined in this study, representing the operational extremes of minimum displacement (light-load condition during outbound transit to fishing grounds) and maximum displacement (heavy-load condition during return voyage with catch and ice). Both loading conditions are evaluated for the baseline hull configuration and for the modified hull incorporating the dihedral bulbous bow, enabling direct performance comparison across the operational displacement range. This approach ensures that hydrodynamic assessment encompasses the full spectrum of realistic operational scenarios.

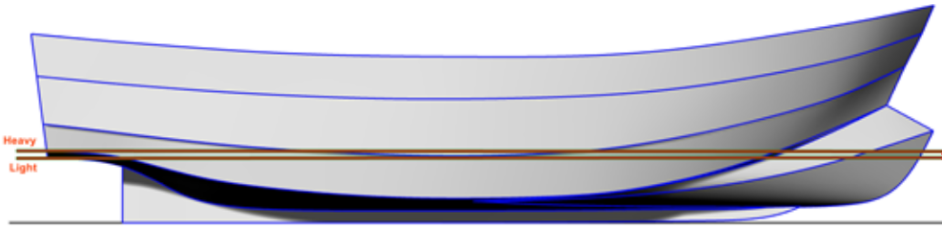

Figure 2. Side view of the vessel showing the dihedral bulbous bow and the reference draft lines for light and heavy loading conditions.

Physical scale models of both hull configurations were fabricated for towing tank testing, as shown in Figure 3. The figure presents the baseline hull model (without bulbous bow) and the modified configuration incorporating the dihedral bow geometry, both constructed at $\lambda = 6.5$ scale for experimental evaluation. These physical models were tested under identical conditions to ensure rigorous performance comparison. The model geometries employed in the experimental programme are geometrically identical to those utilised in the CFD simulations, ensuring consistency between numerical and physical testing and facilitating direct validation of computational predictions against experimental measurements.

(**a**) Original hull model. (**b**) Dihedral bulbous bow model.

Figure 3. Experimental ship models used for towing tank tests.

The principal dimensions and hydrostatic properties of both hull configurations are summarised in Table 2 for the heavy-load and light-load conditions. The table presents comparative data enabling quantification of the geometric and displacement changes resulting from dihedral bow integration, providing the foundation for subsequent hydrodynamic performance analysis.

Table 2. Principal dimensions, hydrostatic particulars, and form coefficients.

	T (m)	$DISP$ (t)	LWL (m)	BWL (m)	A_x (m^2)	AWP (m^2)	C_B	C_X	C_P	C_{WP}
Heavy										
No Bulb	1.200	31.047	13.681	4.402	3.58	47.061	0.42	0.68	0.62	0.78
Bulb	1.200	33.231	14.647	4.402	3.58	48.153	0.42	0.68	0.62	0.75
Light										
No Bulb	1.082	25.624	13.590	4.144	3.07	42.275	0.41	0.68	0.60	0.75
Bulb	1.082	27.661	14.565	4.144	3.07	43.609	0.41	0.68	0.60	0.72

3. Experimental and Numerical Methodology

This investigation employs an integrated experimental and numerical framework combining experimental fluid dynamics (EFD) and computational fluid dynamics (CFD) to comprehensively evaluate the hydrodynamic performance of both hull configurations. The methodology was conceived as a complementary validation and extension strategy: towing tank experiments establish benchmark resistance, trim, and sinkage measurements under controlled conditions, whilst CFD simulations validate these experimental findings and subsequently enable parametric exploration of geometric variations impractical to evaluate through physical model testing. This integrated approach ensures geometric and dynamic consistency between physical models and numerical representations, facilitating comprehensive interpretation of the underlying hydrodynamic phenomena.

3.1. Experimental Setup

The experimental campaign was conducted in the towing tank facility at the Naval Architecture Department of the Technical University of Madrid (ETSIN-UPM), Spain. The basin measures 100 m in length, 3.8 m in width, and 2.2 m in depth—dimensions sufficient to ensure negligible shallow-water and blockage effects at the model scale and test speeds employed. A schematic representation of the facility is presented in Figure 4. The scale model was mounted to the towing carriage through a dynamometric system equipped with guidance arms permitting three degrees of freedom: surge (longitudinal translation), heave (vertical translation), and pitch (rotation about the transverse axis). The remaining degrees of freedom (sway, roll, and yaw) were constrained. Dynamic sinkage and trim angle were continuously monitored using two laser displacement sensors positioned at the forward and aft perpendiculars.

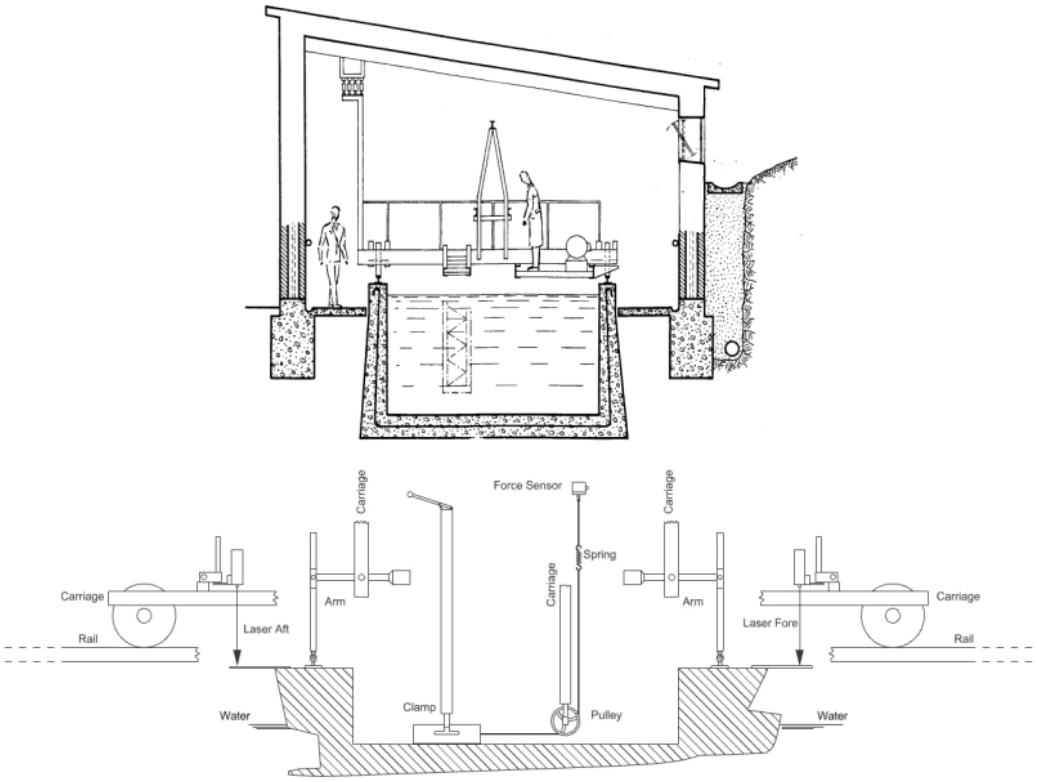

Figure 4. Schematic view of the experimental setup at ETSIN.

Towing resistance was measured using a calibrated Schenck Z6 bending beam load cell mounted to the carriage through a pulley–spring–cable system. The transducer operated at a sampling frequency of 10 Hz and was calibrated over a range exceeding the maximum

anticipated model resistance of approximately 4 kg. Water temperature was monitored throughout testing (16 °C) to enable accurate determination of kinematic viscosity for Reynolds number calculations and full-scale extrapolation following ITTC'78 procedures.

Two loading conditions—heavy-load and light-load—were examined, as illustrated in Figure 2, representing the operational extremes of the vessel's displacement range. Tests were conducted across a speed range from 2 to 10 knots at full scale, corresponding to Froude numbers from approximately 0.08 to 0.42, encompassing the vessel's typical operational envelope from displacement to transitional speed regimes.

3.2. Numerical Setup

Numerical simulations were performed using the open-source finite-volume CFD solver OpenFOAM v12, employing the computational framework established and validated in the authors' previous investigations [1,2,15]. The numerical approach follows best practices for maritime CFD applications, as outlined in recent ITTC-recommended procedures [9] and established reference texts [7]. Turbulence closure was achieved through the Reynolds-averaged Navier–Stokes (RANS) equations coupled with the k–ω shear stress transport (SST) turbulence model. This two-equation eddy-viscosity model was selected for its demonstrated balance between numerical stability and predictive accuracy, particularly in resolving boundary layer flows under adverse pressure gradients and capturing flow separation phenomena characteristic of bluff-body hydrodynamics. The model transitions smoothly between the k–ω formulation in near-wall regions and k–ε behaviour in the outer flow, providing robust predictions across the complete boundary layer thickness. Pressure–velocity coupling was treated using the PIMPLE algorithm, a hybrid procedure combining SIMPLE and PISO approaches that enables larger time steps whilst maintaining solution stability. The free surface between air and water was captured using the volume of fluid (VOF) method with interface compression to maintain sharp phase boundaries and accurately resolve wave profiles.

3.3. Computational Domain and Mesh Generation

The computational domain exploited the longitudinal symmetry plane of the hull, modelling only the starboard half to reduce computational expense whilst maintaining solution accuracy. Predicted forces and moments were subsequently doubled to obtain total values for the complete hull. Domain extents were established following maritime CFD best practices to minimise boundary influence on the flow solution. The hull was positioned three ship lengths ($3L_{PP}$) upstream of the inlet boundary and eight ship lengths ($8L_{PP}$) downstream of the outlet boundary, with lateral and bottom boundaries located at three ship lengths ($3L_{PP}$) from the hull centreline and baseline, respectively. This domain configuration, validated extensively in prior work [1,2], ensures negligible blockage effects and permits full development of the bow wave system, hull boundary layer, and stern wake region.

Mesh generation employed a hierarchical refinement strategy to concentrate computational cells in regions of high flow gradients whilst maintaining efficiency in far-field regions. A baseline Cartesian grid was generated throughout the domain, with successive nested refinement zones progressively halving cell dimensions towards the hull surface and free surface interface. This systematic refinement approach ensures adequate resolution of velocity and pressure gradients within the boundary layer, accurate capture of flow separation at the stern and bulb geometry, and precise representation of the free surface deformation and wave pattern. A schematic representation of the mesh topology and refinement zones is presented in Figure 5.

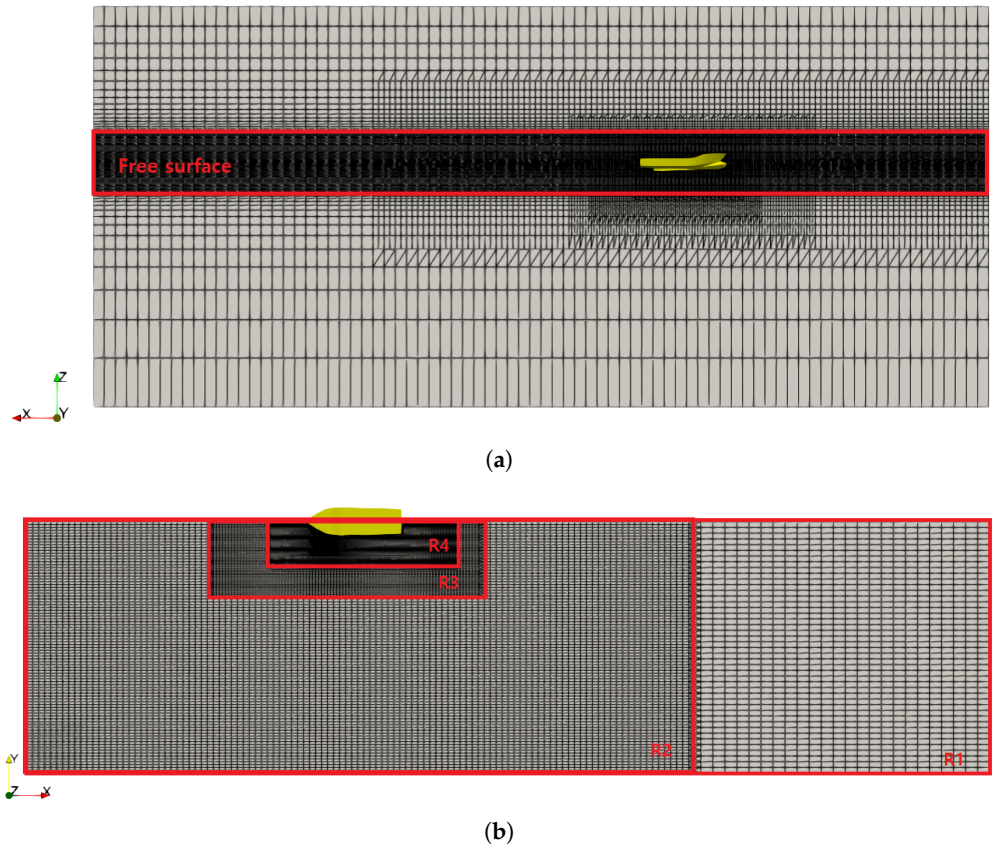

Figure 5. Schematic representation of the mesh and refinement strategy for the computational domain. (**a**): Side view. (**b**): Top view.

The final computational mesh comprised approximately 7 million hexahedral cells, representing an optimised balance between solution accuracy and computational cost. Comprehensive mesh independence studies, grid convergence analyses, and numerical uncertainty quantification following ITTC guidelines have been documented in previous publications employing identical meshing strategies [1,2]. The present investigation therefore focuses on validation of CFD predictions against experimental measurements for the current hull geometries, rather than repeating systematic mesh refinement studies. Grid Convergence Index (GCI) estimates from prior work indicate discretisation uncertainties below 2% for integrated resistance predictions, establishing confidence in the spatial resolution employed [16].

3.4. Validation Strategy and CFD-EFD Integration

All experimental tests and numerical simulations were conducted in calm water conditions, isolating the effects of hull geometry and forward speed without the confounding influences of wave excitation, wind loading, or other environmental disturbances. This approach enables direct attribution of performance differences to the bulbous bow modification rather than to external factors.

The parallel deployment of towing tank experiments and CFD simulations enables rigorous cross-validation of results through direct comparison of resistance, trim, and sinkage predictions against measured values. Agreement between EFD and CFD establishes confidence in the numerical predictions and validates the computational framework for subsequent parametric investigations. Once validated against experimental benchmarks, the CFD methodology was employed to explore additional geometric configurations, loading conditions, and speed ranges beyond those evaluated experimentally, thereby extending the scope of hydrodynamic assessment without the time and cost constraints of

physical model testing. This validation-then-extension strategy reinforces the applicability and reliability of the proposed methodology for evaluating future vessel modifications and retrofit design optimisation.

4. Results

This section presents the hydrodynamic performance results obtained through combined experimental testing in the towing tank facility and numerical simulation using OpenFOAM v12. The presentation follows a structured validation-then-analysis approach: CFD predictions are first validated against experimental measurements for each parameter before proceeding to detailed analysis and presentation of additional quantities accessible only through numerical simulation. This methodology ensures that numerical predictions of experimentally challenging quantities—such as vertical lift forces and resistance component decomposition—are established on a foundation of validated computational accuracy.

4.1. Hydrodynamic Force Analysis

The analysis of hydrodynamic forces constitutes a critical element in assessing bulbous bow retrofit feasibility. From a practical standpoint, the primary criterion for bulbous bow implementation is whether the modification yields substantial reductions in required propulsive power, as such reductions translate directly to decreased fuel consumption and operational costs—providing compelling economic incentive for vessel operators to undertake the retrofit investment.

4.1.1. Total Resistance

Total resistance represents the most operationally significant hydrodynamic parameter, as it directly governs installed power requirements, fuel consumption, emissions intensity, and overall economic viability of vessel operation. This analysis compares resistance characteristics between the baseline hull configuration and the modified hull incorporating the dihedral bulbous bow across the operational speed range.

Validation of the numerical methodology against experimental measurements was conducted as the foundation for subsequent analyses of quantities not directly measurable experimentally, including resistance component decomposition (viscous and pressure contributions), vertical lift forces, and detailed pressure field distributions. These numerical results provide essential information for identifying the operational speed regime where the bulbous bow becomes effective and for quantifying the magnitude of performance improvement under both loading conditions for this displacement-type vessel.

Figures 6 and 7 present quantitative validation of CFD predictions against experimental measurements for the light-load and heavy-load conditions, respectively, encompassing both the baseline hull and the dihedral bulb configuration. The comparison demonstrates close agreement between numerical and experimental data across the speed range, with mean deviations not exceeding 5%. This level of accuracy establishes confidence in the CFD methodology for subsequent parametric investigations and analysis of quantities not directly measurable through experimentation.

Figure 8 presents comparative resistance characteristics for both loading conditions across the model-scale speed range from 2 to 10 knots at full scale. The results reveal a consistent pattern: below approximately 7 knots, resistance values for the baseline and modified configurations remain essentially identical, with differences falling within experimental uncertainty. Beyond this critical threshold speed, however, the dihedral bulb configuration consistently exhibits lower resistance than the baseline hull for both loading conditions.

Under light-load conditions, a maximum resistance reduction of approximately 18% is achieved at 9 knots with the dihedral bulb installation. For the heavy-load condition, maximum bulb effectiveness occurs at 7 knots—two knots lower than the light-load case—suggesting displacement-dependent performance characteristics. Significantly, the bulb becomes effective precisely within the speed range (7–10 knots) where resistance increases most rapidly and where the vessel typically operates during transit to and from fishing grounds. This operational alignment enhances the practical value of the retrofit, as fuel consumption is highest during these high-speed transit phases.

The results demonstrate that substantial calm water resistance reduction can be achieved through dihedral bulb integration without any modification to the parent hull lines—a critical consideration for retrofit applications where extensive structural alteration is economically prohibitive.

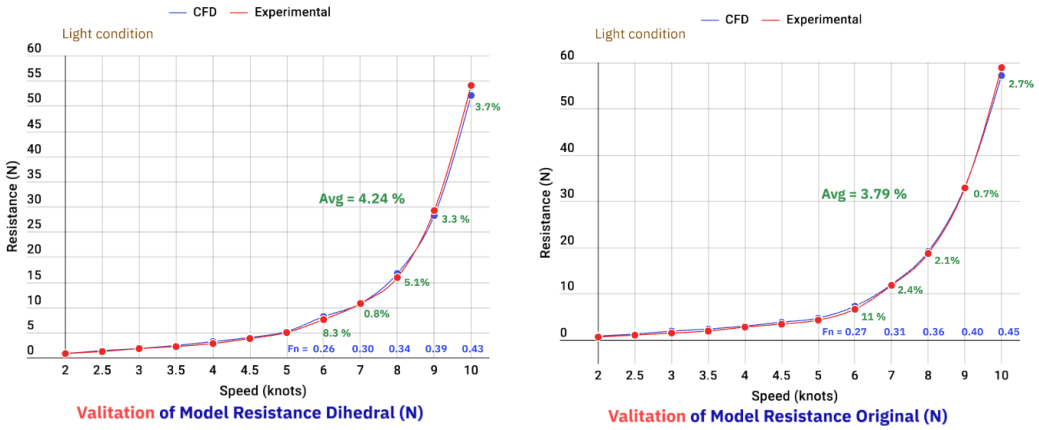

Figure 6. Validation of CFD vs. EFD resistance curves under light condition: (**a**) validation of model resistance—dihedral configuration; (**b**) validation of model resistance—original configuration.

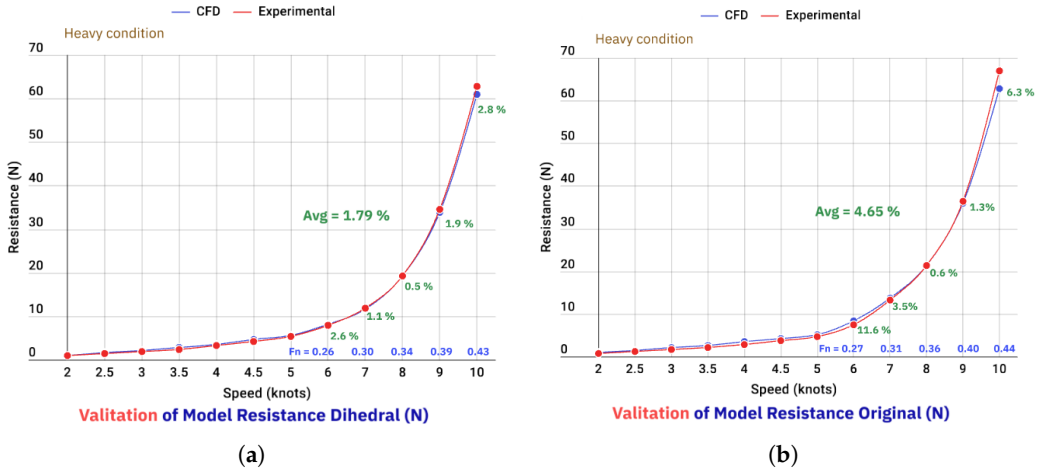

Figure 7. Validation of CFD vs. EFD resistance curves under heavy condition: (**a**) validation of model resistance—dihedral configuration; (**b**) validation of model resistance—original configuration.

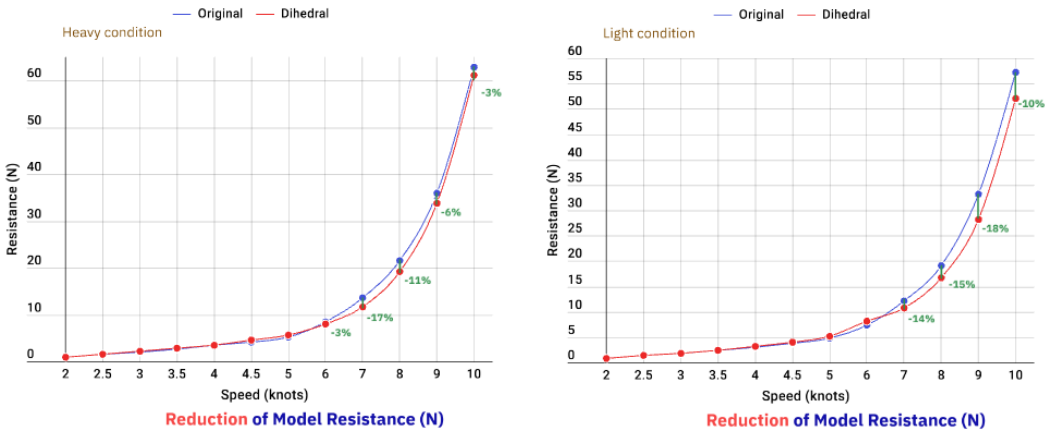

(**a**) (**b**)

Figure 8. Drag comparison between original and dihedral configurations: (**a**) original vs. dihedral for heavy condition and (**b**) original vs. dihedral for light condition.

4.1.2. Pressure Resistance Component

Numerical simulation enables decomposition of total resistance into viscous (friction) and pressure (form + wave-making) components, facilitating identification of the physical mechanisms responsible for the observed resistance reduction. This subsection examines the pressure resistance component, whilst the viscous component is addressed subsequently in Section 4.1.3. This analysis clarifies whether the bulbous bow primarily reduces pressure-related resistance or viscous resistance, providing insight into the dominant hydrodynamic mechanism.

Figure 9 presents pressure resistance for both loading conditions across the speed range. For both light-load and heavy-load cases, a critical transition occurs near 6 knots. Below this speed, pressure forces remain nearly identical for both hull configurations, with absolute magnitudes remaining relatively small and exhibiting minimal variation between configurations. Beyond this critical speed, however, a pronounced divergence emerges: the dihedral bulb configuration exhibits substantially lower pressure resistance than the baseline hull for both loading conditions.

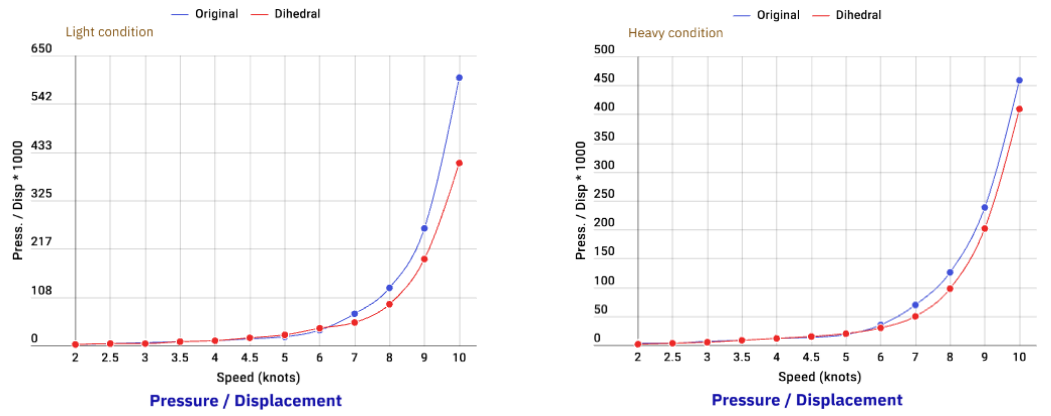

(**a**) (**b**)

Figure 9. Pressure-to-displacement ratio versus speed for the original and dihedral configurations under light and heavy loading conditions: (**a**) light condition and (**b**) heavy condition.

This behaviour correlates directly with the onset of significant wave-making resistance, which becomes the dominant resistance component at higher Froude numbers. The bulb becomes hydrodynamically effective precisely at the speed where wave-making resistance

begins to dominate, confirming that the primary resistance reduction mechanism operates through favourable wave interference and modified bow pressure distribution rather than through viscous effects.

4.1.3. Viscous Resistance Component

Figure 10 presents the viscous (frictional) resistance component of total resistance. Conventional expectations would suggest that integration of an additional geometric element such as a bulbous bow should increase wetted surface area and consequently increase viscous resistance. The results, however, demonstrate that this penalty does not materialise: for both light-load and heavy-load conditions, viscous resistance remains essentially unchanged across the entire speed range investigated.

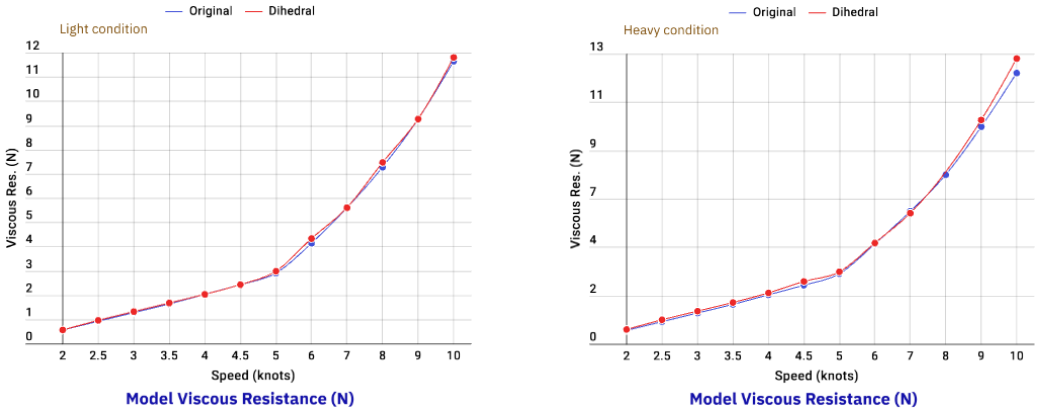

Figure 10. Model viscous resistance versus speed for the original and dihedral configurations under light and heavy loading conditions: (**a**) light condition and (**b**) heavy condition.

Consequently, the observed total resistance reduction derives almost entirely from decreased pressure resistance, whilst the viscous component remains unaffected by dihedral bulb integration. This represents a substantial advantage, as viscous resistance typically dominates at lower speeds and often increases significantly when bulbous bows are added due to wetted surface area enlargement. The present results confirm that the dihedral bulb configuration achieves resistance reduction exclusively through pressure field modification and wave interference effects, without incurring viscous resistance penalties. This favourable characteristic likely results from the surface-piercing geometry of the dihedral bulb, which minimises additional submerged surface area compared with conventional fully submerged bulb configurations.

4.1.4. Vertical Lift Forces

This subsection examines the vertical hydrodynamic forces acting on both hull configurations under light-load and heavy-load conditions. Vertical lift forces are of particular significance, as they govern dynamic trim equilibrium and influence resistance through trim-induced changes in wetted surface area and running attitude. These forces are accessible only through numerical simulation, as direct experimental measurement of vertical forces was not conducted in the present towing tank programme.

Figure 11a presents lift force characteristics for the light-load condition, comparing the baseline and dihedral configurations. Both configurations exhibit essentially constant lift from 2 knots to approximately 5–6 knots, beyond which behaviour diverges significantly. This speed represents a critical transition threshold where hydrodynamic lift begins to develop substantially.

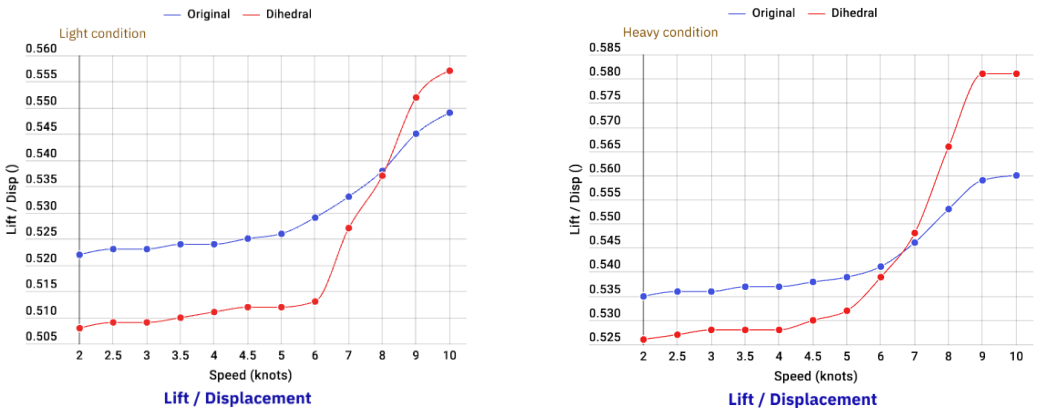

Figure 11. Lift comparison under (**a**) Lift comparison for light condition and (**b**) Lift comparison for heavy condition.

For the dihedral configuration, lift exhibits exponential growth beyond 6 knots, such that, by 8 knots, the lift force equals that of the baseline hull, and exceeds it at 9 and 10 knots. In contrast, the baseline configuration exhibits lift increase commencing around 5–6 knots, but developing in a more gradual linear manner compared with the exponential growth observed with the dihedral bulb. This behaviour indicates that the dihedral bow generates progressively greater dynamic lift as speed increases, which produces significant effects on trim angle evolution, as discussed subsequently in Section 4.2.

For the heavy-load condition, presented in Figure 11b, a similar trend is observed up to 5 knots, where both configurations exhibit nearly constant lift magnitudes. Beyond this threshold, the dihedral configuration demonstrates exponential increase in vertical force, reaching a pronounced maximum at 9 knots before stabilising at 10 knots. The baseline configuration, conversely, exhibits more gradual linear increase commencing around 6 knots, stabilising between 9 and 10 knots at an approximately constant value. This behaviour corresponds directly to the speed regime where significant trim changes occur. Particularly under conditions where lift forces reach maximum values (8–10 knots), the trim response in the dihedral configuration is markedly more pronounced than in the baseline hull.

These results indicate that the bulbous bow substantially modifies the vertical force distribution and alters the hydrodynamic load spectrum experienced by the hull. Although the vessel operates predominantly in the displacement regime, the changes induced by the dihedral configuration not only affect trim behaviour but also modify the pressure-induced structural loads acting on the bow region, which may have implications for local structural strength assessment. The trim changes induced by bulb-generated vertical forces subsequently influence resistance through modification of the hull's running attitude and wetted surface distribution.

4.2. Dynamic Trim Analysis

This section examines the dynamic trim behaviour of both hull configurations across the operational speed range. Figures 12 and 13 present validation of CFD-predicted trim angles against experimental measurements for light-load and heavy-load conditions, respectively. Visual comparison indicates satisfactory agreement between experimental and numerical data, with both datasets exhibiting consistent trends in trim angle evolution with speed, establishing confidence in the numerical predictions of trim behaviour.

Figure 14a presents CFD-predicted trim behaviour comparing the dihedral bulb and baseline configurations under light-load conditions. Both hulls exhibit similar trim charac-

teristics up to approximately 6 knots, beyond which behaviour diverges progressively. For the hull fitted with the dihedral bulb, trim angle becomes increasingly negative (bow-down trim), reaching maximum bow-down attitude around 8–9 knots. This speed range coincides precisely with the regime of maximum resistance reduction discussed previously.

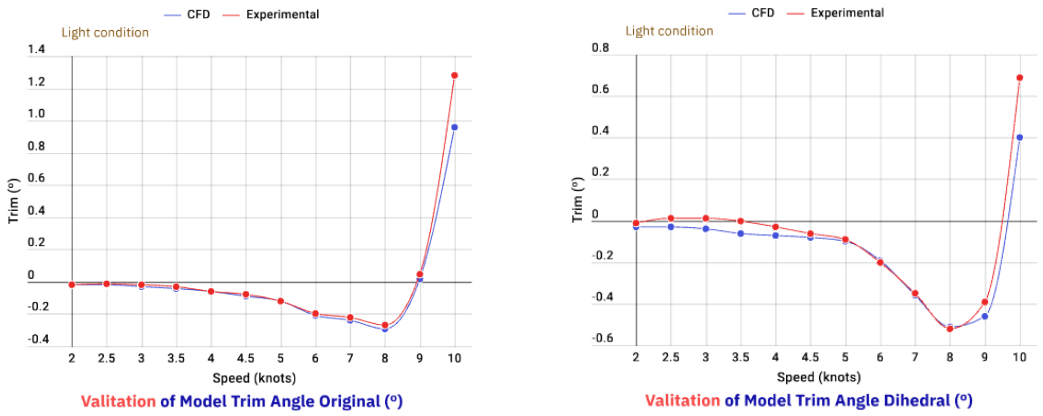

(**a**) (**b**)

Figure 12. Trim angle validation for light condition: (**a**) Trim angle validation for light condition and original hull. (**b**)Trim angle validation for light condition and dihedral bow.

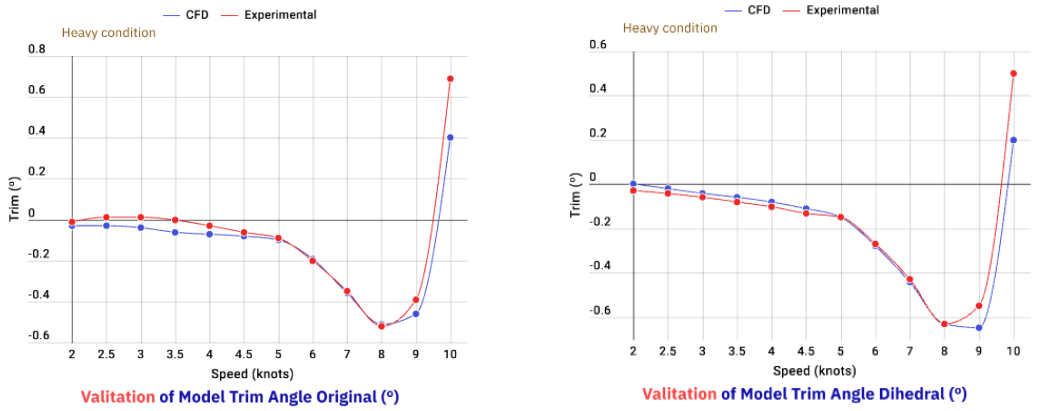

(**a**) (**b**)

Figure 13. Trim angle validation for heavy condition: (**a**) Trim angle validation for heavy condition and original hull. (**b**) Trim angle validation for heavy condition and dihedral bow.

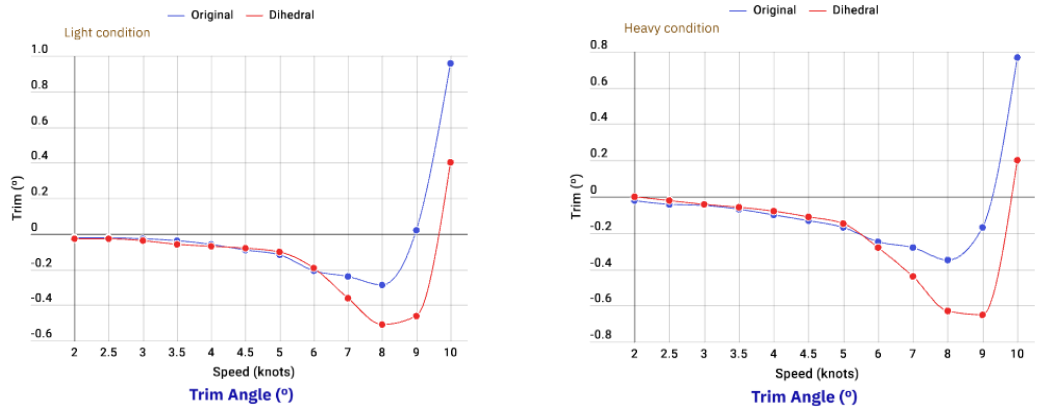

(**a**) (**b**)

Figure 14. Trim angle comparison under (**a**) Trim angle for light condition comparison. (**b**) Trim angle for heavy condition comparison.

This correlation suggests a dual mechanism of resistance reduction in the dihedral configuration: first, direct reduction through favourable wave interference and pressure field modification attributable to the bulb geometry itself, and second, indirect reduction through trim-induced decrease in effective angle of attack and wetted surface distribution. The bow-down trim induced by increased forward lift generation reduces the stern immersion and decreases the wetted transom area, both of which contribute to resistance reduction. This finding is particularly significant, as it reveals that the bulb operates through complementary hydrodynamic mechanisms rather than through a single effect.

For the heavy-load condition, shown in Figure 14b, similar trends are observed. Both configurations follow closely aligned trim angles up to approximately 6 knots, after which progressive divergence occurs. The maximum difference in trim angle between configurations is observed near 9 knots, consistent with the light-load case. This confirms that as speed increases beyond the critical threshold, the hull fitted with the dihedral bulb consistently achieves greater bow-down trim reduction compared with the baseline hull, substantially affecting resistance characteristics and reinforcing the observed performance improvements.

5. Experimental Flow Visualisation

Figures 15–20 present photographic evidence from towing tank tests comparing the baseline and dihedral bulb configurations at 6, 8 and 10 knots. These visualisations illustrate how the bulb presence modifies wave generation patterns along the hull surface. In both loading conditions, the bulb acts to smooth the water entry flow onto the hull, effectively attenuating the bow wave system that, in the baseline hull, exhibits noticeably larger amplitude and steeper wave profiles.

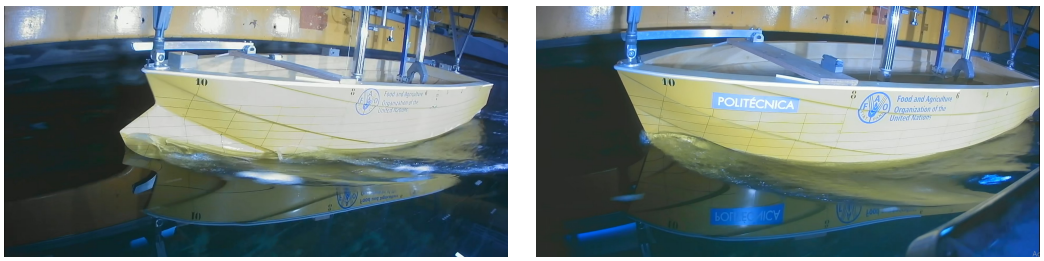

(**a**) (**b**)

Figure 15. Experimental towing tank tests comparing the original FAO fishing vessel model with the modified hull fitted with a dihedral bulbous bow at 6 knots and light load condition: (**a**) model with dihedral bulbous bow during towing tank tests and (**b**) original model without bulbous bow during towing tank tests.

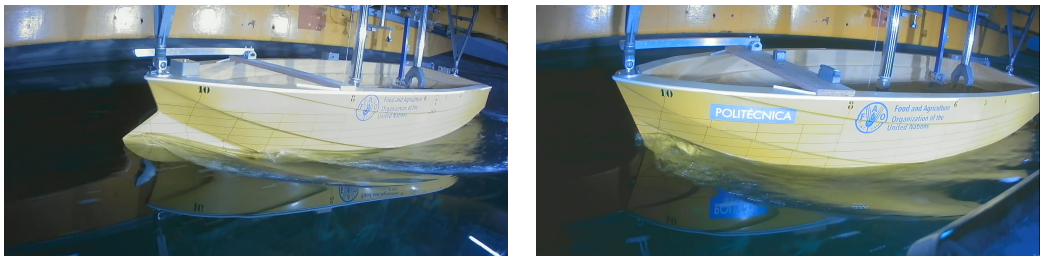

(**a**) (**b**)

Figure 16. Experimental towing tank tests comparing the original FAO fishing vessel model with the modified hull fitted with a dihedral bulbous bow at 6 knots and heavy load condition: (**a**) model with dihedral bulbous bow during towing tank tests and (**b**) original model without bulbous bow during towing tank tests.

(a) (b)

Figure 17. Experimental towing tank tests comparing the original FAO fishing vessel model with the modified hull fitted with a dihedral bulbous bow at 8 knots and light load condition: (**a**) model with dihedral bulbous bow during towing tank tests and (**b**) original model without bulbous bow during towing tank tests.

(a) (b)

Figure 18. Experimental towing tank tests comparing the original FAO fishing vessel model with the modified hull fitted with a dihedral bulbous bow at 8 knots and heavy load condition: (**a**) model with dihedral bulbous bow during towing tank tests and (**b**) original model without bulbous bow during towing tank tests.

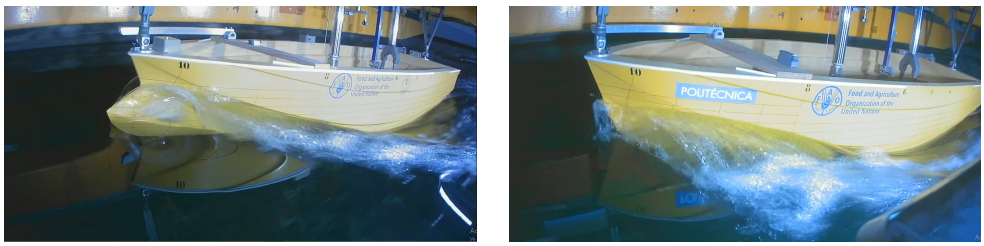

(a) (b)

Figure 19. Experimental towing tank tests comparing the original FAO fishing vessel model with the modified hull fitted with a dihedral bulbous bow at 10 knots and light load condition: (**a**) model with dihedral bulbous bow during towing tank tests and (**b**) original model without bulbous bow during towing tank tests.

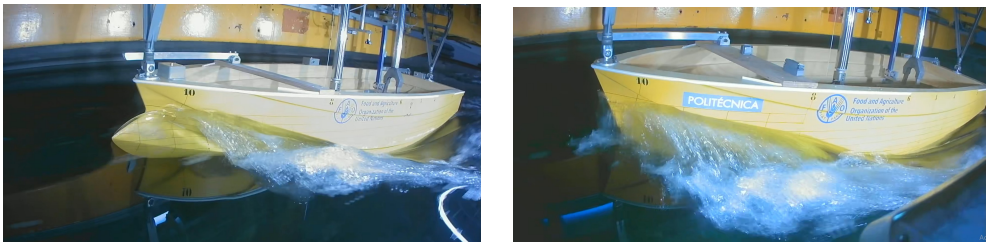

(a) (b)

Figure 20. Experimental towing tank tests comparing the original FAO fishing vessel model with the modified hull fitted with a dihedral bulbous bow at 10 knots and heavy load condition: (**a**) model with dihedral bulbous bow during towing tank tests and (**b**) original model without bulbous bow during towing tank tests.

The dihedral bulb configuration produces an effective elongation of the hydrodynamic entrance length, thereby softening the water entry process. This is achieved by providing a more gradual angle of attack as the bulb progressively cuts through the water ahead of the parent hull bow, leading to more distributed flow around the forward sections. This behaviour differs markedly from that reported in Reference [1], where a deeply submerged bulb configuration was investigated, whereas the present surface-piercing dihedral geometry operates at the waterline interface, producing distinctly different flow modification mechanisms.

On the other hand, the wave generation observed in some experiments can be attributed to the effects induced by attack angle and hull speed, as can be seen, for instance, in the 10-knot case. For the different operating conditions—namely, 10, 8, and 6 knots—it is observed that the local wave depth at the wave crest, particularly at the midship section, varies as a function of how the flow is distributed around the hull. This behaviour is also reflected in the longitudinal elongation of the wave pattern and in the position along the hull where the generated wave reaches its maximum amplitude.

For example, in the 10-knot cases, the wave is generated at different longitudinal locations depending on the configuration, and the resulting wave amplitude differs noticeably between the bulbous bow and non-bulbous bow cases. Furthermore, when considering different draft conditions, it can be observed that the bulb interacts with the water in a distinct manner, effectively modifying the wave-cutting process and leading to either higher or lower generated wave amplitudes.

As expected, when the hull is more deeply submerged, the resulting wave tends to exhibit greater prominence. This is due to the increased water displacement and the larger volume of water that must be displaced by the bulb. Consequently, a deeper and more pronounced wave is formed around the midship region, which in turn leads to a different velocity flow distribution along the hull.

Full-Scale Extrapolation and Practical Implementation

The results obtained in this investigation extend beyond academic contribution to practical engineering application: based on the favourable model-scale findings discussed in preceding sections, the dihedral bulb retrofit has been implemented on a full-scale operational vessel. Figure 21a shows the vessel in its original as-built configuration without bulbous bow, whilst Figure 21b presents the final retrofitted configuration incorporating the dihedral bulb geometry validated through the present research programme.

(**a**) (**b**)

Figure 21. Comparison of the vessel configurations: (**a**) original vessel and (**b**) vessel fitted with the dihedral bulbous bow.

Full-scale implementation requires prior analysis of the resistance reduction expected at full scale, as the evaluations conducted thus far were performed at model scale under Froude scaling. Consequently, extrapolation of model-scale results to full-scale predictions has been conducted following ITTC'78 guidelines [9], representing established best practice

for resistance prediction and power estimation in naval architecture. The analysis presented herein quantifies the effective power reduction achieved through bulb integration as a function of vessel speed at full scale.

Determination of full-scale effective power (EHP) requires extrapolation of model-scale resistance data using the ITTC resistance decomposition methodology. Prohaska [17] proposed an experimental approach for estimating the form factor $(1 + k)$, which is regarded as the most reliable method and is recommended by the ITTC [18]. This procedure assumes that for Froude numbers below 0.2, the wave resistance coefficient (C_W) can be approximated by αFn^4. Under this assumption, Equation (2) can be reformulated for model tests as

$$\frac{C_{TM}}{C_{FM0}} = (1 + k) + \alpha \frac{Fn^4}{C_{FM0}} \quad (1)$$

where C_{FM0} denotes the ITTC-57 correlation line friction coefficient evaluated at the model Reynolds number, whilst C_{TM} represents the dimensionless total resistance coefficient of the model.

The ITTC method for decomposing the total resistance coefficient (C_T) is based on Hughes's hypothesis [19] and introduces the form factor k, which augments the flat-plate friction coefficient to account for three-dimensional hull form effects on the boundary layer. Accordingly, the total coefficient can be expressed as

$$C_T = (1 + k)C_{F0} + C_W \quad (2)$$

In this expression, $(1 + k)C_{F0}$ corresponds to the viscous resistance coefficient (C_V), whilst C_W denotes the wave resistance coefficient. The viscous component comprises the flat-plate friction coefficient (C_{F0}) and the additional influence of hull form on boundary layer development, represented as a multiplicative factor $(1 + k)$ applied to the friction coefficient [18]. Further details regarding extrapolation in the fishing vessel field are provided in [20].

Following the extrapolation procedure described above, the effective power (EHP) is calculated in kilowatts, representing the propulsive power requirement for hull towing without consideration of propeller efficiency or transmission losses. Figure 22a presents the extrapolated full-scale power comparison under light-load conditions. It is important to note that the percentage resistance reduction attributable to the bulb at full scale is somewhat lower than that observed at model scale when compared with the baseline hull due to scale effects on the viscous-wave resistance ratio. For this reason, presentation of full-scale extrapolated results is essential, as they provide substantially more accurate prediction of real-world operational performance.

Under light-load conditions, substantial resistance reduction is observed from 7 knots onwards when compared with the baseline hull. The reduction commences at approximately 15% at 7 knots, reaches a maximum of 20% at 8 knots, remains at approximately 15% at 9 knots, and diminishes to approximately 10% at 10 knots. These reductions translate to significant absolute power savings during high-speed transit operations.

For the heavy-load condition, shown in Figure 22b, resistance reduction is also evident, though of smaller magnitude than in the light-load case. The bulb effect initiates at 7 knots with a reduction of approximately 14%, decreasing progressively to approximately 7% at 10 knots. Nevertheless, even this reduced benefit remains operationally significant: a 7% power reduction at 10 knots corresponds to absolute power savings between 6 and 9 kW EHP, which accumulates to substantial fuel cost savings over extended operational periods typical of fishing voyages.

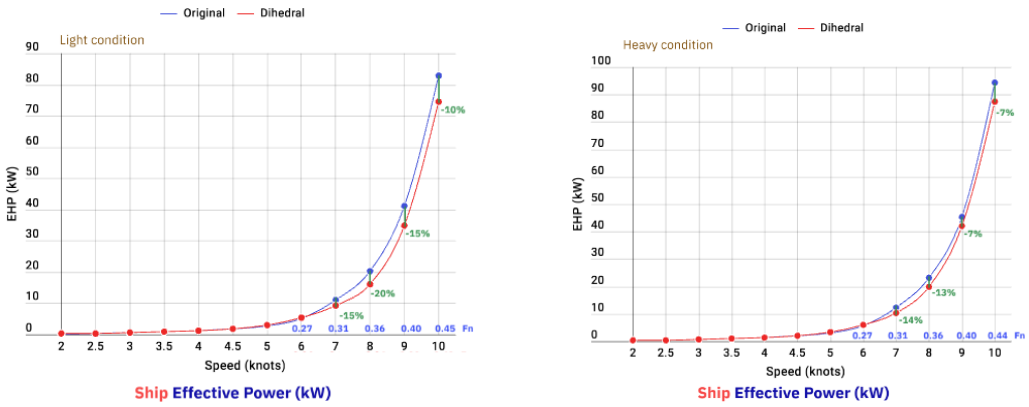

(**a**) (**b**)

Figure 22. Comparison of EHP full-scale results in light and heavy conditions: (**a**) EHP full-scale light condition and (**b**) EHP full-scale heavy condition.

6. Discussion

This investigation has demonstrated that integration of a surface-piercing dihedral bulbous bow onto the FAO longliner fishing vessel hull yields substantial hydrodynamic performance improvements across the operational speed range. The combined experimental and numerical study establishes that resistance reduction becomes effective beyond a critical threshold of approximately 6 knots (Fr ≈ 0.25), with maximum savings reaching 18–20% under light-load conditions and approximately 14% under heavy-load conditions. Force decomposition analysis reveals that this resistance reduction derives primarily from decreased pressure resistance attributable to favourable wave interference and modified bow pressure distribution, whilst viscous resistance remains essentially unaffected by bulb integration—a particularly advantageous characteristic, as it avoids the wetted surface penalties typically associated with appendage additions.

Beyond direct resistance reduction, the dihedral bulb substantially influences vertical lift force generation and dynamic trim behaviour, producing complementary performance enhancement mechanisms. The bulb generates increased forward lift at speeds above 6 knots, inducing bow-down trim that reduces stern immersion and wetted transom area, thereby contributing additional resistance reduction beyond the direct hydrodynamic effects of the bulb geometry itself. This dual mechanism—combining direct pressure field modification with indirect trim-induced improvements—distinguishes the dihedral configuration from conventional fully submerged bulbous bows.

Extrapolation of model-scale results to full scale following ITTC'78 guidelines confirms that the observed performance benefits transfer effectively to full-scale vessels, yielding substantial reductions in effective power requirements across the operational speed range. Under light-load conditions, power savings range from 15% at 7 knots to 20% at 8 knots, diminishing to 10% at 10 knots. Even under heavy-load conditions, where benefits are more modest, power reductions of 7–14% are achieved at speeds of 7 to 10 knots—representing absolute savings of 6–9 kW that accumulate to significant fuel cost reductions over typical fishing voyage durations.

The successful full-scale implementation of the dihedral bulb retrofit on an operational vessel validates the design methodology and demonstrates the practical feasibility of this intervention. The surface-piercing dihedral geometry offers particular advantages for retrofit applications: the developable surface construction simplifies fabrication using conventional boatbuilding techniques accessible to small shipyards, whilst the waterline-emergent configuration minimises additional wetted surface and associated viscous penalties. These characteristics render the dihedral bulb retrofit especially suitable for small

fishing vessels under 20 metres in length, where modest efficiency improvements yield disproportionate economic benefits due to the high proportion of operational costs attributable to fuel consumption.

The demonstrated hydrodynamic advantages translate directly to operational and environmental benefits: fuel consumption reductions of 10–20% during high-speed transit phases correspond to proportional decreases in greenhouse gas emissions, contributing to the decarbonisation objectives increasingly mandated for maritime operations. For artisanal fishing fleets comprising hundreds or thousands of vessels based on similar hull forms, widespread adoption of dihedral bulb retrofits could yield substantial aggregate emissions reductions without requiring fleet replacement or alternative propulsion system investments.

Several avenues for future research merit consideration. The present investigation was conducted exclusively in calm water conditions; evaluation of seakeeping performance in representative sea states would provide complementary assessment of wave-induced motions, slamming loads, and operational behaviour in realistic fishing conditions. Systematic parametric optimisation of bulb geometry—including longitudinal position, immersion depth, sectional area distribution, and chine line configuration—could potentially yield further performance improvements beyond the single geometry evaluated herein. Full-scale operational trials with instrumented measurement of fuel consumption under realistic fishing operation profiles would provide definitive validation of predicted fuel savings and enable comprehensive economic payback analysis.

The present investigation contributes to the broader body of work on hull form optimisation and energy efficiency enhancement in maritime vessels. As outlined in recent ITTC reports [9,10], systematic approaches combining experimental validation with numerical parametric studies represent the current state of practice for vessel performance prediction and design optimisation. The validated methodology employed herein aligns with these recommended practices and demonstrates their applicability to small fishing vessel retrofit applications, an area of increasing importance for maritime decarbonisation efforts.

In conclusion, the dihedral bulbous bow retrofit represents a practical, cost-effective, and environmentally beneficial intervention for enhancing the operational efficiency of small displacement-type fishing vessels. The surface-piercing developable geometry achieves substantial resistance reduction through favourable pressure field modification without incurring viscous penalties, whilst the dual mechanism of direct and trim-induced improvements maximises performance benefits. The validated design methodology and successful full-scale implementation establish confidence in this retrofit approach as a viable strategy for improving the sustainability and economic viability of artisanal fishing operations.

Conclusions Overview

The following points summarise the principal findings of the present investigation, highlighting the dominant hydrodynamic mechanisms, performance gains, and practical implications of the dihedral bulbous bow retrofit for small displacement-type fishing vessels.

- Integration of a surface-piercing dihedral bulbous bow produces significant hydrodynamic performance improvements for the FAO longliner hull, becoming effective above a critical speed of approximately 6 knots (Fr $\approx$ 0.25).
- Maximum resistance reductions of 18–20% are achieved under light-load conditions, and approximately 14% under heavy-load conditions, with savings driven primarily by reduced pressure resistance due to favourable wave interference. Viscous resistance remains largely unaffected, avoiding wetted-surface penalties.

- The dihedral bulb induces increased forward vertical lift at higher speeds, generating bow-down trim that reduces stern immersion and wetted transom area, providing additional resistance reduction through indirect trim effects.
- Full-scale extrapolation following ITTC'78 procedures confirms effective transfer of model-scale benefits, yielding power savings of 15–20% under light-load conditions and 7–14% under heavy-load conditions.
- The surface-piercing, developable geometry is well suited for retrofit applications, enabling simple fabrication with conventional shipyard techniques whilst minimising additional wetted surface.
- Fuel consumption reductions of 10–20% during transit phases translate directly into proportional greenhouse gas emission reductions, offering a cost-effective decarbonisation pathway for small fishing vessels under 20 m in length.

Author Contributions: H.R.D.O.: validation, investigation, funding acquisition, writing—original draft, writing—review; Y.Z.: validation, investigation, writing—original draft; S.T.: investigation, writing—original draft, writing—review; F.P.A.: conceptualisation, investigation, funding acquisition, writing—review, supervision. All authors have read and agreed to the published version of the manuscript.

Funding: This document is the results of the research project funded by the Spanish Ministry of Ciencia e Innovación through grant PID2022-140481OB-I00.

Data Availability Statement: The original contributions presented in this study are included in the article. Further inquiries can be directed to the corresponding authors.

Acknowledgments: The authors acknowledge the use of the IRIDIS High Performance Computing Facility, and associated support services at the University of Southampton, in the completion of this work. The authors also acknowledge the funding provided by the Ministerio de Ciencia e Innovación through grant PID2022-140481OB-I00. FAO, with support from the Norwegian government-funded trust fund project GCP/GLO/352/NOR, introduced the bulbous bow as a fuel-saving exercise in 2023.

Conflicts of Interest: The authors declare no conflicts of interest.

Nomenclature

Symbol	Definition
LOA	Length Overall
Lpp	Length between Perpendiculars
Lwl	Length on Waterline
BOA	Breadth Overall
T	Draft
DISv	Displacement Volume
DISM	Displacement Mass
S	Wetted Surface Area
CG	Center of Gravity

References

1. Díaz-Ojeda, H.; Pérez-Arribas, F.; Turnock, S.R. The influence of dihedral bulbous bows on the resistance of small fishing vessels: A numerical study. *Ocean Eng.* **2023**, *281*, 114661. [CrossRef]
2. Pérez-Arribas, F.; Silva-Campillo, A.; Díaz-Ojeda, H.R. Design of Dihedral Bows: A New Type of Developable Added Bulbous Bows—Experimental Results. *J. Mar. Sci. Eng.* **2022**, *10*, 1691. [CrossRef]
3. Calisal, S.; Mikkelsen, J.; Mcgreer, D. Resistance Tests with UBC Series Fishing Vessels. In Proceedings of the SNAME 23rd American Towing Tank Conference, New Orleans, LA, USA, 11–12 June 1992. [CrossRef]
4. Ali, A.; Peng, H.; Qiu, W. Resistance prediction of two fishing vessel models based on RANS solutions. *Phys. Chem. Earth Parts A/B/C* **2019**, *113*, 115–122. [CrossRef]

5. Liang, J.; Tan, W. Comparative experimental research on fishing vessel's bulbous bow model in resistance reduction and energy conservation. *Fish. Mod.* **2009**, *36*, 54–58.
6. Leksono, S.; Muryadin; Kartikasari, D. Comparative Study of Ship Resistance between Model Test and Empirical Calculation of 60 GT Fishing Vessel. *Int. J. Sci. Res.* **2018**, *7*, 1077–1082.
7. Molland, A.F.; Turnock, S.R.; Hudson, D.A. *Ship Resistance and Propulsion: Practical Estimation of Ship Propulsive Power*, 2nd ed.; Cambridge University Press: Cambridge, UK, 2017.
8. Bahatmaka, A.; Kim, D.J. Numerical Approach for the Traditional Fishing Vessel Analysis of Resistance by CFD. *J. Eng. Sci. Technol.* **2019**, *14*, 207–217.
9. ITTC. Recommended Procedures and Guidelines: Resistance Test. In Proceedings of the 30th International Towing Tank Conference, Tasmania, Australia, 22–27 September 2024.
10. ITTC. Recommended Procedures and Guidelines: Energy Efficient Ship Design and Operation. In Proceedings of the 30th International Towing Tank Conference, Tasmania, Australia, 22–27 September 2024.
11. Bilec, M.; Obreja, C. Ship Resistance and Powering Prediction of a Fishing Vessel. *IOP Conf. Ser. Mater. Sci. Eng.* **2020**, *916*, 012011. [CrossRef]
12. Food and Agriculture Organization of the United Nations. FAO Fisheries and Aquaculture—Vessel Design Database (Search). 2025. Available online: https://www.fao.org/fishery/en/vesseldesign/search (accessed on 9 September 2025).
13. Food and Agriculture Organization of the United Nations. FAO Fisheries and Aquaculture—Vessel Design Collection. 2025. Available online: https://www.fao.org/fishery/en/collection/vesseldesign (accessed on 9 September 2025).
14. Food and Agriculture Organization of the United Nations. FAO Fisheries and Aquaculture—Vessel Design: SRI-15. 2025. Available online: https://www.fao.org/fishery/en/vesseldesign/sri-15 (accessed on 9 September 2025).
15. Díaz Ojeda, H.R.; Oyuela, S.; Sosa, R.; Otero, A.D.; Pérez Arribas, F. Fishing Vessel Bulbous Bow Hydrodynamics—A Numerical Reverse Design Approach. *J. Mar. Sci. Eng.* **2024**, *12*, 436. [CrossRef]
16. Oyuela, S.; Ojeda, H.R.D.; Arribas, F.P.; Otero, A.D.; Sosa, R. Investigating Fishing Vessel Hydrodynamics by Using EFD and CFD Tools, with Focus on Total Ship Resistance and Its Components. *J. Mar. Sci. Eng.* **2024**, *12*, 622. [CrossRef]
17. Prohaska, C. A simple method for evaluation of the form facter and low speed wave resistance. In Proceedings of the 11th ITTC, Tokyo, Japan, 10–20 October 1966; pp. 65–66.
18. 26th ITTC Resistance Committee. *ITTC—Recommended Procedures and Guidelines—Resistance Test*; ITTC: Hannover, Germany, 2011.
19. Hughes, G. Friction and form Resistance in Turbulent Flow, and a Proposed Formulation for Use in Model and Ship Correlation. *RINA Trans.* **1954**, *96*, 314–376.
20. Oyuela, S.; Díaz-Ojeda, H.R.; Otero, A.D.; Sosa, R. Combined CFD-EFD methods applied to determining the form factor of vessels with very low length to beam ratio. *Ocean Eng.* **2026**, *352*, 124211. [CrossRef]